

Estimation of Basin Parameters and Precipitation Distribution of Solakli Basin, Turkey

SEZEL KARAYUSUFOGLU

Department of Satellite Communication and Remote Sensing

Istanbul Technical University

34469 Maslak, Istanbul

TURKEY

sezel.karayusufoglu@gmail.com

EBRU ERIS

Department of Civil Engineering

Istanbul Technical University

34469 Maslak, Istanbul

TURKEY

eriseb@itu.edu.tr

H. GONCA COSKUN

Department of Geomatic Engineering

Istanbul Technical University

34469 Maslak, Istanbul

TURKEY

gonca@itu.edu.tr

Abstract: - Solakli Basin is located Eastern Black Sea region where high mountain ranges run parallel to the coast in the north. Such a mountainous terrain, it is generally hard or impossible to reach to acquire data by terrestrial measurement. However, today, by using integration of Remote Sensing and Geographic Information Systems even those kinds of basins can be modelled. These techniques provide to derive basin, land use and/or soil type characteristics in an accurate and quick way, particularly for water resources assessment studies. In addition to basin characteristics, spatial distribution of precipitation is also important for these types of studies.

In this study, for the classification of Solakli Basin IRS P6 multispectral satellite data with 5.8 m spatial resolution are used and to derive the Digital Elevation Model IRS P5 stereo satellite data with 2.5 m spatial resolution is used. The basin characteristics are mathematically determined. Isohyetal maps to understand precipitation distribution are generated by means of different geostatistical methods such as Inverse Distance Weight, Radial Basis Function and Kriging. Among these methods, Kriging and Radial Basis Function give more satisfactory results.

Key-Words: -Basin characteristics, Remote Sensing, GIS, Classification, Image Processing, Geostatistical methods.

1 Introduction

It is getting indispensable to explore and research the Earth in the fastest and the cheapest way due to the growing population, violated natural reserves, effects of global climate changing, disasters causing distractions. Admitted, efficient and useful way to detect, manage and analyse earth surface is the integration of Remote Sensing (RS) and Geographic Information System (GIS). In comparison to the conventional methods integrated work of RS and GIS offer faster and economical solutions. Recently, for the hydrology and water resource studies and researches, RS and GIS are being used. Furthermore with the power of the recent advances in computer science and technology scientists, engineers and managers employ these two effective tools, the RS and the GIS, to obtain the needed parameters for the possible hydrological models. In combination with appropriate hydrological models, the RS and GIS provide ideal tools for the estimation of direct runoff volume, peak flows and hydrographs [1; 2; 3, 4, 5]. Generally, RS data provide a source of input parameters for the models in stream flow estimation. Thematic information on land use, soil, vegetation, drainage, etc., and topographic parameters (area, elevation and slope) which combined with conventionally measured climatic parameters (precipitation, temperature, etc.), constitute the necessary input data for the rainfall-flow models are provided by satellite data. Using high resolution satellite imagery, Digital Elevation Model (DEM) and land cover maps can be obtained. Information can be provided in a quick, accurate and reliable way compared to classical terrestrial survey methods. In GIS media, RS data and other information, can be stored as geographically referenced [6; 7; 8]. DEM is produced using stereo satellite images and digital topographic maps and used for determination of the elevation, slope, and aspect information of the basin. Additionally, processing the DEM data in a specific software module, area of each subbasins and synthetic drainage network data can be derived. In GIS environment the whole information can be combined with hydro-meteorological data [9; 10; 11]. Integrated RS and GIS studies have been used in water resources assessment in the literature and these studies provide more practical and less time consuming results [12; 13; 14].

The precipitation distribution also plays significant role for the hydrological models or water resources projects such as dam and hydroelectric power plant (HPP) constructions. For mountainous and poorly gauged basins precipitation prediction is a difficult and time consuming process. Different methods have been developed to predict the distribution of precipitation in such basins, using limited point-scale precipitation data. Geostatistical methods such as Inverse Distance Weight, Radial Basis Function, Kriging etc., is one of these

methods. These methods have been widely used by many researchers [15; 16; 17].

In this study, DEM of a poorly gauged stream basin, Solakli, is generated and basin characteristics are obtained by using RS and GIS. To determine spatial distribution of precipitation of the basin, various geostatistical methods are performed and isohyetal maps are generated.

2 Study Area and Data

The study area, Solakli Basin is placed in the city of Trabzon at the Eastern Black Sea Region and located at $41^{\circ} 00'$ North latitude and $39^{\circ} 43'$ East longitude (Fig.1). It covers an area of 767.25 km^2 . Haldizen and Soganli Mountains rise in the south part of the basin where the highest point Demirkapi Hill reaches to 3376 m elevation. Solakli stream is the main stream of the basin. Especially during the spring, both snow covering starts to melt and the severe convectional activities in the atmosphere causes heavy precipitation lead floods and landslides. Dense forest cover also a considerable factor results in difficulties for the conventional terrestrial measurements.

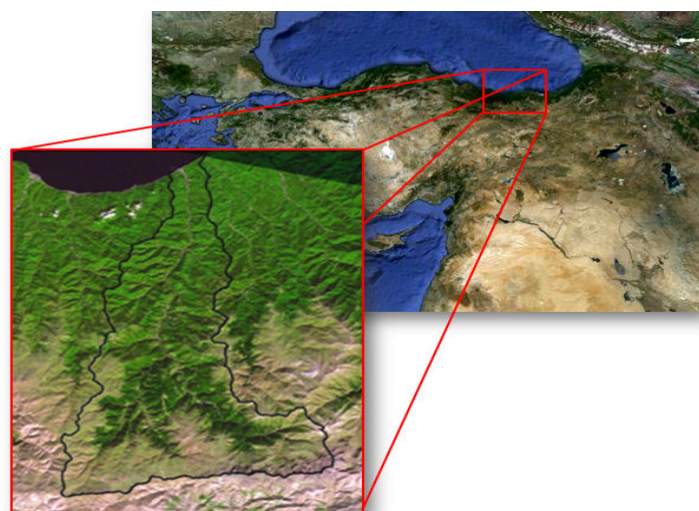


Fig.1 Study area

Stereo Cartosat - 1 (IRS P5) satellite data (Fig.2) with 2.5 meter spatial resolution (Table 1) is used for DEM derivation procedure.

There are only three precipitation gauging stations available in Solakli Basin. To generate more accurate isohyetal map for Solakli Basin, precipitation stations which are located Eastern Black Sea Region are used. Location of 38 precipitation stations can be seen in Fig.3. For the validation stage six precipitation stations are randomly chosen. Table 2 shows the characteristics of these stations.

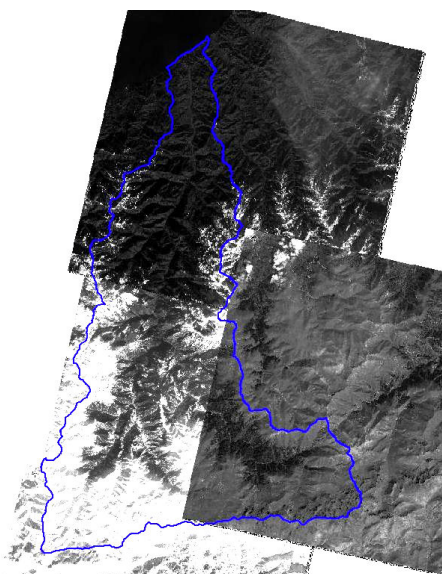


Fig.2 Pre-image of the study area from Cartosat 1 (IRS P5) satellite on 18.12.2006.

Table 1 Characteristics of Stereo Cartosat - 1 (IRS P5) satellite

	PAN-Fore	PAN-Aft
Tilt Along Track	+26 deg	-5 deg
Spatial Resolution	2.5 m	2.5 m
Swath-width	30 km	27 km
Radiometric Resolution, Quantisation	10 bit	10 bit
Spectral Coverage	500-850nm	500-850nm
Focal Length	1945 mm	1945 mm
CCD Arrays (no. of arrays * no. of elements)	1 * 12000	1 * 12000
CCD Size	7 μ m x 7 μ m	7 μ m x 7 μ m
Integration Time	0.336 ms	0.336 ms

Mean annual precipitation data record length ranges from 10 to 46 years; however, there are some gaps in the data. To complete the gap in any gauge record, regression equations were developed using continuous data from the nearby gauges. The homogeneity of the data was first checked out with the double mass curve method. Trend analysis was also made with the Mann-Kendall trend test [18].

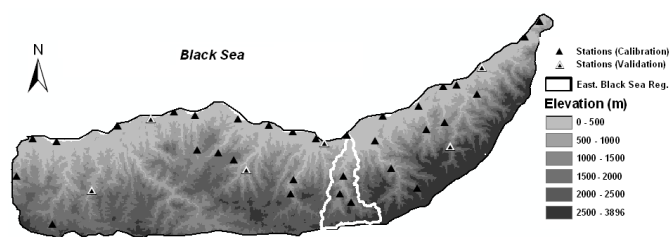


Fig.3 Precipitation gauging stations used to generate isohyetal map.

Table 2 Precipitation stations for validation stage

Station Name	Coordinates (m)		Elevation (m)
	X	Y	
Gorele	500000	4542457	20
Surmene	594327	4529502	12
Findikli	680093	4570589	100
Sinir	467607	4503676	750
Macka	552032	4514888	300
Meydan	662887	4527605	1100

3 Basin Characteristics and Classification

3.1 Determination of basin characteristics

DEM is produced in order to determine the topographic parameters of Solakli Basin.

Automated stereo correlation has become a standard method for generating DEMs from digital stereo images. Automatic image matching is the basis of the stereo correlation. Although approaches may vary according to the software employed, the procedures normally include the collection of Ground Control Points (GCPs), determination of parallax values on a per pixel or per DEM post basis using automatic image matching techniques and, finally, post-processing to remove the anomalies from the DEMs [19].

Using dual frequency GPS instruments, 65 GCPs based on 11 points from National Network Stations are collected in order to generate DEM. Accuracy of these points reaches ± 10 cm (Fig.4a) after processing the collected data. Using GCPs measured with static GPS equipment and the tie points collected from the stereo pairs an absolute DEM with 5 m cell size is generated (Fig.4b, c). Both in planimetric position and elevation, the expected accuracy of the DEM is approximated to be 4 m.

DEM should be cleared of pits or ponds, where water gathers when drainage network is extracted, before being used in the hydrological modelling [20]. Using an algorithm known as sink filling a sign of errors, pits, can be removed from DEMs. After removing the errors by filling sinks algorithm, by calculating the steepest slope and by encoding into each cell for possible eight flow

directions toward the surrounding cells a flow direction map is produced (Fig.5a) [7].

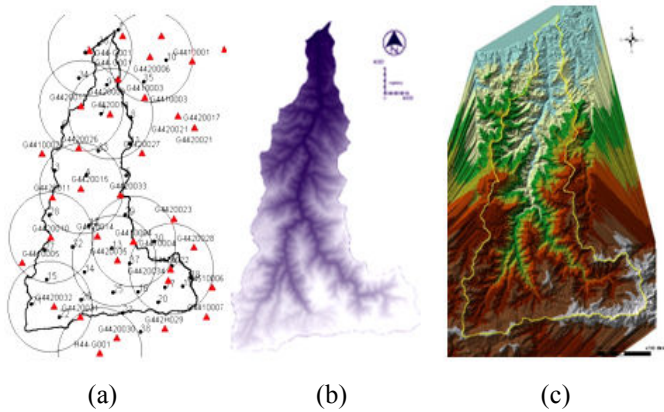


Fig.4 (a) Static stations used in GPS measurements; (b); (c) Generated DEM

Then flow direction is used to produce the flow accumulation map by addressing each cell of the DEM, counting how many upstream cells contribute to flow through the given cell (Fig. 5b). After all, both flow accumulation and flow direction maps are used to create synthetic drainage network of the basin (Fig. 5c).

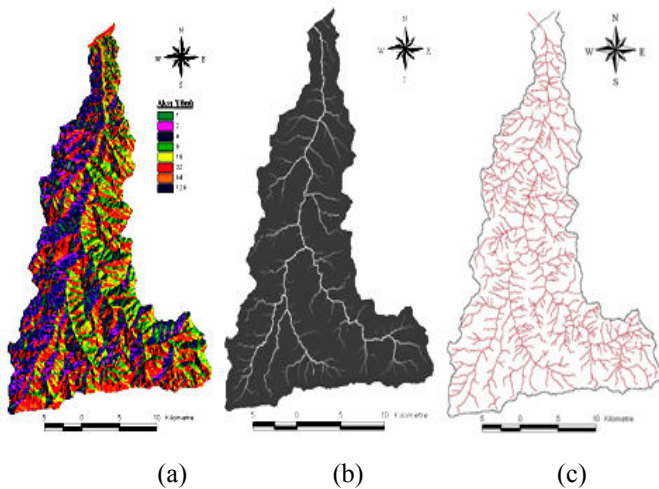


Fig.5 (a)Flow direction map; (b) Flow accumulation map; (c) Synthetic drainage network of the basin.

3.2 Image Prossessing

Images geometrically might have some distortions that are caused by systematic or non-systematic errors due to the changes of the sensors platform height, location or velocity and curvature of the Earth's surface. It is provided by removing those distortions, that satellite images can be integrated to the map geometry. Fig. 6 shows geometrically corrected satellite image.

IRS P6 Multispectral – Panchromatic data set, with 23m and 5.8m spatial resolution, respectively, is merged using IHS Transform (Fig.7) in order to obtain high

spatial and radiometric resolution image (Fig.8). Technical information of the IRS P6 satellite is shown at Table 3.

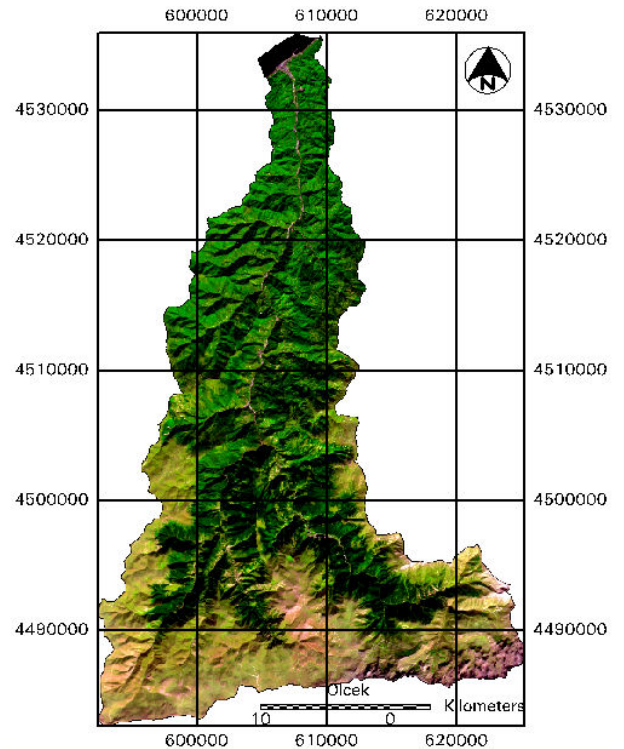


Fig.6 Geometrically corrected satellite image.

Table 3 Characteristics of the IRS P6 Satellite.

IRS – P6 (LISS IV)		LISS-IV		LISS-III
		Mono Mode	MX Mode	
Spatial Resolution	All bands	5.8 m	5.8 m	23.5 m
Frame Width	All bands	70 km	23.9 km	140 km
Radiometric Resolution	All bands	7 bit	7 bit	7 bit
Spectral Resolution	Band2 (green) Band3 (red) Band4 (NIR) Band5 (SWIR)	620-680nm	520-590nm 620-680nm 770-860 nm	520-590 nm 620-680 nm 770-860 nm 1550-1700 nm

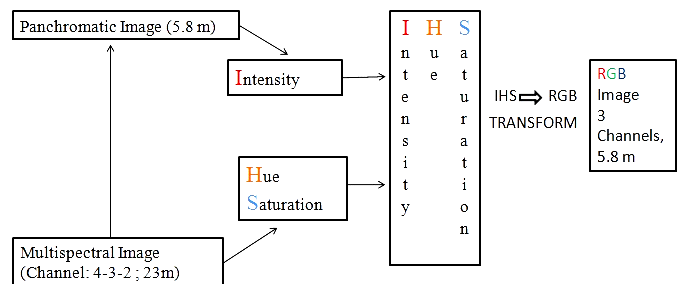


Fig.7 IHS Transform.

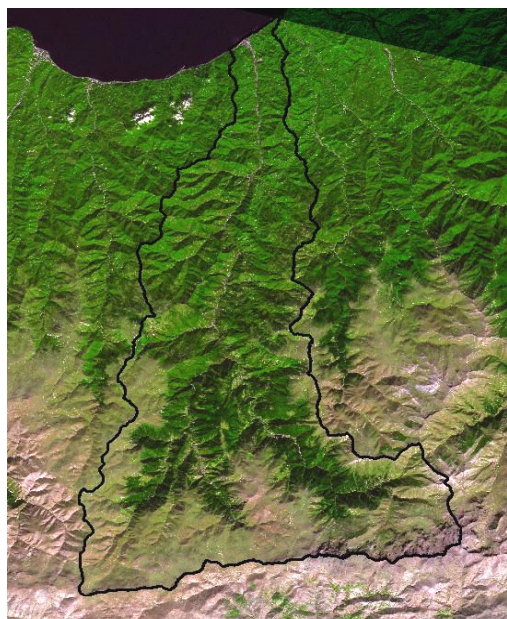


Fig.8 IRS P6 image after IHS Transform that is used for classification.

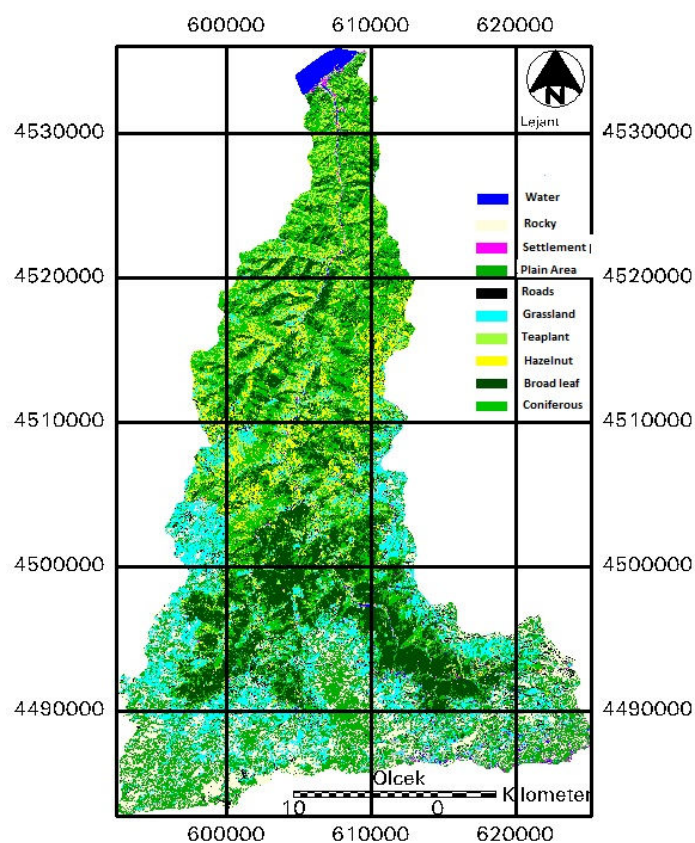


Fig.9 Classified image.

3.3 Image Classification

The rectified and merged image is subjected to a classification procedure with ten classes, using the supervised Maximum Likelihood Classification algorithm. These ten classes were verified using pattern recognition, referring to the ground truth data and fieldwork. The classification results are evaluated in an accuracy assessment. In this accuracy assessment 100 random pixels are chosen and these pixels compared with the results of the fieldwork. Accuracy assessment results are 80.00%.

From the RS analysis, it is found that the basin area consists of 22.6% coniferous forest area, 20.4% broadleaf forest area, 1.2% water covered surface, 1.4% settlement area, 12.2% rocky area, 15.8% plain area, 0.5% roads, 13.9% grassland, 4.6% tea plant covered area and hazel-nut area covers 7.4% of the total basin area (Fig. 9).

4 Precipitation Distribution

In the literature several interpolation techniques for sparse data have been discussed. On the other hand, geostatistical techniques are progressively more preferred because they allow one to capitalize on the spatial structure/correlation between neighbouring observations to predict attribute values and to quantify prediction uncertainty at unsampled locations [15]. In this study, to create the isohyetal map using mostly preferred geostatistical methods such as Inverse Distance Weight, Radial Basis Function and Kriging.

4.1 Inverse Distance Weight (IDW)

IDW interpolation explicitly implements the assumption that things that are close to one another are more alike than those that are farther apart. To predict a value for any unmeasured location, IDW will use the measured values surrounding the prediction location. Those measured values closest to the prediction location will have more influence on the predicted value than those farther away. Thus, IDW assumes that each measured point has a local influence that diminishes with distance. The general equation for the inverse distance weighted method is

$$z_o = \frac{\sum_{i=1}^s z_i \frac{1}{d_i^k}}{\sum_{i=1}^s \frac{1}{d_i^k}} \quad (1)$$

where, z_o is the estimated value at point 0, z_i is the z value at control point i , d_i is the distance between control point i and point 0, s is the number of control points used in estimations and k is the specified power. A low power (<2) results in a greater contribution towards a grid point value of precipitation from distant gauges, indicating a low spatial variability and vice versa.

The optimal power value is determined by minimizing the root mean square prediction error (RMSE). The RMSE is the statistic that is calculated from cross-validation. RMSE can be calculated as:

$$RMSE = \sqrt{\frac{1}{n} \sum_1^n (P_{est} - P_{obs})^2} \quad (2)$$

where, P_{obs} and P_{est} represent observed and estimated precipitation values.

To search the most appropriate number of neighbours, in this study, various neighbour numbers are tried. The most appropriate neighbor number is chosen based on the lowest RMSE value (Fig.10).

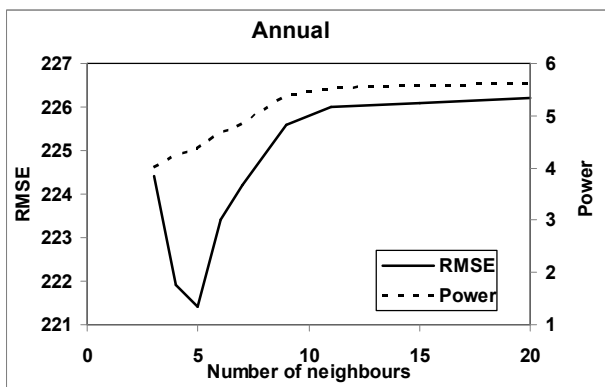


Fig.10 Determination number of neighbours and power value.

4.2 Radial Basis Funtion (RBF)

RBF methods are a series of exact interpolation techniques; that is, the surface must go through each measured sample value. There are five different basis functions:

- Thin-plate spline
- Spline with tension
- Completely regularized spline

- Multiquadric function
- Inverse multiquadric function

The predictor is a linear combination of the basis functions,

$$\hat{Z}(s_o) = \sum_{i=1}^n \omega_i \phi(|s_i - s_o|) + \omega_{n+1} \quad (3)$$

where, $\phi(r)$ is a radial basis function, Euclidean distance between the prediction location s_o and each data location s_i , and $\{\omega_i: i=1,2,\dots, n+1\}$ are weights to be estimated. Each basis function has a different shape and results in a slightly different interpolation surface. RBF methods are a form of artificial neural networks.

To select the most appropriate basis function, RMSE values are determined from the cross validation results. In this study, Spline with tension function generally gives the lowest RMSE value for the precipitation data (Fig.11). Because of this, Spline with tension function is chosen to generate isohyetal maps for RBF method.

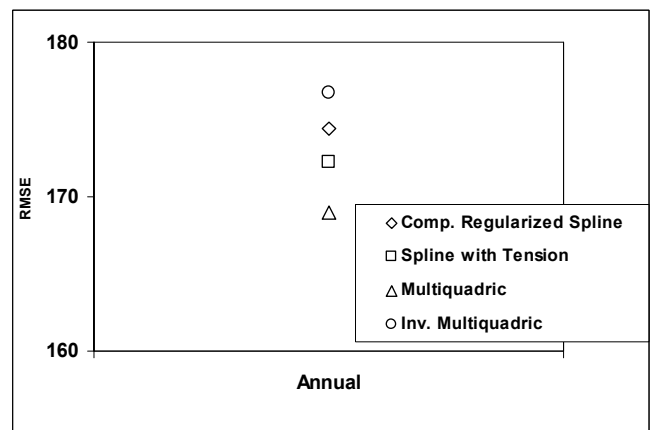


Fig.11 Comparison of RMSE values of different basis functions.

4.3 Kriging

In brief, Kriging is based on the estimated spatial covariance structure of the observed data and implemented as two- or three-dimensional interpolation technique [21; 22].

Let x_1, x_2, \dots, x_n be the sample locations with given precipitation values of $Z(x_1), Z(x_2), \dots, Z(x_n)$ and x_0 is the unsampled location. Then the value of precipitation in the unsampled location, $Z(x_0)$, is estimated as a linear weighted combination of n known surrounding data, depending on distance from the unsampled location:

$$Z^*(x_0) = \sum_{i=1}^N \lambda_i Z(x_i) \quad i = 1,2,\dots,n \quad (4)$$

where the weights λ_i are determined such that $Z^*(x_0)$ is an unbiased estimate of $Z(x_0)$:

$$E[Z^*(x_0) - Z(x_0)] = 0 \tag{5}$$

and the estimation variance is minimum:

$$E[Z^*(x_0) - Z(x_0)]^2 \rightarrow \text{minimum} \tag{6}$$

where $E[.]$ is the expectation. Substituting equation (6) into equations (7) and (8) yields:

$$E\left[\sum_{i=1}^n \lambda_i Z(x_i) - Z(x_0)\right] = 0 \tag{7}$$

$$E\left[\sum_{i=1}^n \lambda_i Z(x_i) - Z(x_0)\right]^2 \Rightarrow \text{minimum} \tag{8}$$

The optimal weights λ_i are solutions of the following linear system, called the Kriging system:

$$\begin{aligned} \sum_{i=1}^n \lambda_i C(x_i, x_j) + \mu &= C(x_i, x_j) \\ \sum_{i=1}^n \lambda_i &= 1 \end{aligned} \tag{9}$$

where $C(x_i, x_j) = E[Z(x_i)Z(x_j)]$ is the covariance and μ is a Lagrange multiplier which was employed to obtain the weights.

In the kriging system the estimation variance is written in terms of differences between two sample locations.

The minimization yields the replacement of $C(x_i, x_j)$ by $\gamma(x_i, x_j)$:

$$\sum_{i=1}^n \lambda_i \gamma(x_i, x_j) + \mu = \gamma(x_i, x_j) \sum_{i=1}^n \lambda_i = 1 \tag{10}$$

which yields the semi-variogram equations:

$$\gamma(h) = \frac{1}{2} E[(Z(x+h) - Z(x))^2] \tag{11a}$$

or

$$\gamma(h) = \frac{1}{2} \text{var}(Z(x+h) - Z(x)) \tag{11b}$$

$\gamma(h)$ is the semi-variogram function, h is the distance between sample locations (also called the lag) and $\text{var}(-)$ is the variance. The semi-variogram $\gamma(h)$ is a graph which relates the differences or increments of the

regionalized variable Z to the distance h between the data points. There are several types of kriging:

- Simple Kriging
- Ordinary (Punctual) Kriging
- Universal Kriging
- Indicator Kriging
- Disjunctive Kriging
- Cokriging

In this study ordinary type of kriging is used for the map. For such high altitude areas, the ordinary kriging method does not seem to be the best for precipitation distribution but relationship between precipitation and altitude varies over the entire region, co-kriging may not lead to improvement of results [23]. Incorporation of elevation data for precipitation estimation is beneficial when the value of correlation coefficient between precipitation and elevation is larger than 0.75 [15, 24, 25]. With a correlation coefficient of 0.51, co-kriging was not considered appropriate for this study (Fig.12).

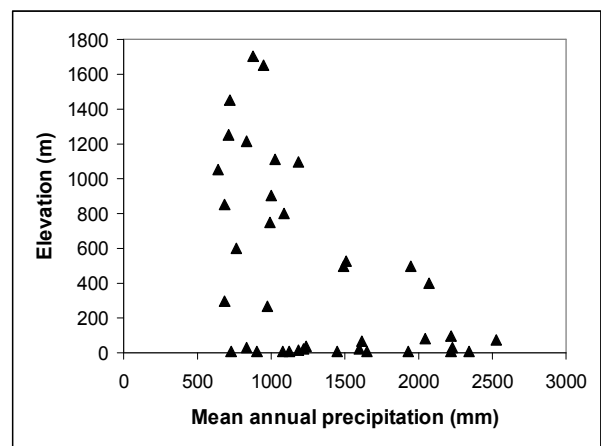


Fig.12 Relationship between precipitation and elevation.

4.4 Results

Mean annual total precipitation data from 38 rain gage stations of Eastern Black Sea Region were used to derive isohyetal map for Solakli Basin. The accuracy of aforementioned interpolation methods was obtained by means of cross validation technique. In this technique, each data is removed one at a time, and then is predicted from the remaining data using the selected method. This procedure is repeated for a second point, and so on. For all points, cross-validation compares the measured and predicted values. Cross validation results of methods are shown in Fig. 13 with determination coefficient (R^2). The determination coefficient is a measure of goodness of fit provided by the selected method. R^2 values close to one would imply that the model can explain most of the variation in the dependent variable and in turn shows how convenient the model is.

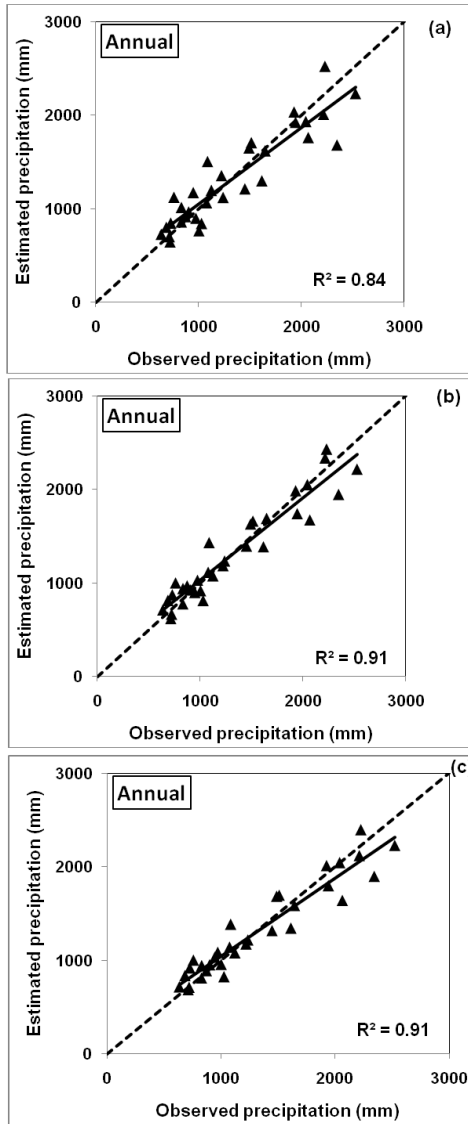


Fig.13 Cross validation results for (a) IDW, (b) RBF and (c) Kriging.

As seen from Fig.13, R^2 values of three models appears to be satisfactory, however, RBF and Kriging methods give better cross validation results than that of IDW. Isohyetal maps generating using IDW, RBF and Kriging methods were presented in Fig.14, Fig.15, Fig.16, respectively. Isohyetal maps confirm the cross validation results that maps using by RBF and Kriging are similar to each other but differ from that of IDW.

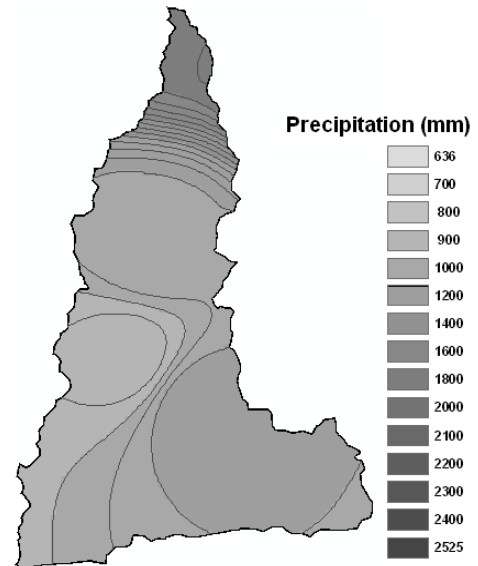


Fig.14 Isohyetal map using IDW.

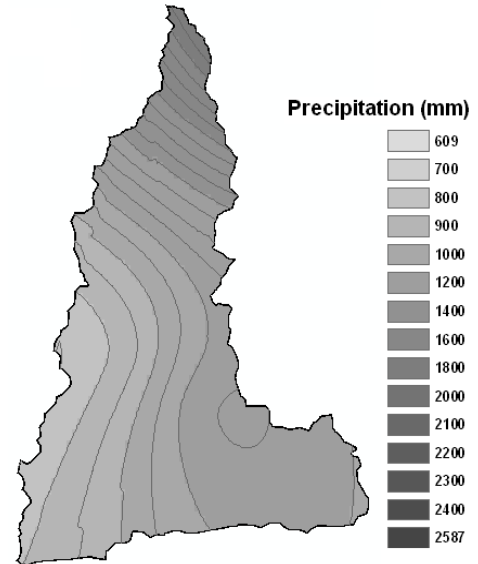


Fig.15 Isohyetal map using RBF.

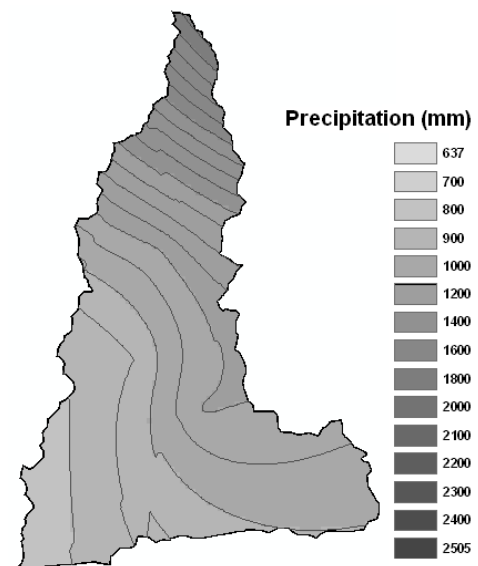


Fig.16 Isohyetal map using Kriging.

Table 4 shows the relative errors for the stations which were chosen for the validation stage. RE is computed using:

$$RE = \frac{P_{est} - P_{obs}}{P_{obs}} \times 100 \quad (5)$$

where P_{est} and P_{obs} are the estimated and observed precipitations in precipitation gauges, respectively

Table 4 Results for validation stations

	Relative Errors (%)		
	IDW	RBF	Kriging
Gorele	-8.9	<u>-2.35</u>	-6.12
Surmene	-8.1	-1.89	<u>-0.56</u>
Findikli	-12.0	-7.39	<u>-6.30</u>
Sinir	<u>7.3</u>	13.60	12.47
Macka	4.3	5.88	<u>2.72</u>
Meydan	27.6	<u>1.01</u>	9.76

The validation results appear satisfactory, particularly for RBF and Kriging. Minimum and maximum relative errors are -12.0 and 27.6 respectively for IDW, whereas these are -7.39 and 13.6 for RBF and -6.30 and 12.47 for Kriging.

5 Conclusion

In this study, Remote Sensing and GIS co-work provided basin characteristics for a mountainous and poorly gauged Solakli basin. The employment of the GIS and RS techniques for the basin parameter determination is a quite useful way especially for a mountainous terrain for which it is generally hard or impossible to reach to acquire data by terrestrial measurement.

In addition, spatial distribution of precipitation for Solakli basin is determined for water resources assesment or a possible hydrological model. Isohyetal maps to understand precipitation distribution are generated by means of different geostatistical methods such as Inverse Distance Weight, Radial Basis Function and Kriging. Among these methods, Kriging and Radial Basis Function give more satisfactory results.

References:

[1] Bellal, M., Sillen, X., Zeck, Y., 1996, Coupling GIS with a distributed hydrological model for studying the effect of various urban planning options on rainfall-runoff relationship in urbanised basins. In: K. Kovar, and H. P. Nachtnebel, (ed) Application of Geographic Information Systems in hydrology and water resources management: International Association of Hydrological

Sciences, Series of Proceedings and Reports. 235: 99-106.

[2] Demayo, A. and Steel, A., 1996, Data handling and presentation. In: D. Chapman, (ed). Water quality assessments, a guide to the use of biota, sediments and water in environmental monitoring: London, United Nations Educational, Scientific and Cultural Organization, World Health Organization, United Nations Environment Programme, 2nd edition. 10: 511-612.

[3] Miloradov, M., Marjanovic, P., 1991, Geographic Information System in environmentally sound river basin development. 3rd Rhine-Danube Workshop. 7-8 October Delft the Netherlands Technische Universiteit Delft.

[4] Dudhani, S., Sinha, A. K., Inamdar, S. S., 2006, Assessment of small hydropower potential using Remote Sensing data for sustainable development in India. Energy Policy, 34: 3195-3205.

[5] Abdelkader M., Mohamed E., Abdelkader D., 2007, Hydrologic model combined to a GIS for estimating hydrologic balance at watershed scale - Application to the watershed of Macta (Western Algerian), Proceedings of the 2nd IASME / WSEAS International Conference on Water Resources, Hydraulics & Hydrology, Portoroz, Slovenia, May 15-17, pp26-30.

[6] Rouhani H., Feyen J., Willems P., 2006, Impact of watershed delineations on the SWAT runoff prediction: a case study in the Grote Nete catchment, Proceedings of the 2006 IASME/WSEAS Int. Conf. on Water Resources, Hydraulics & Hydrology, Chalkida, Greece, May 11-13, pp36-41.

[7] Hammouri, N., El-Naqa, A., 2007, Hydrological modeling of ungauged wadis in arid environments using GIS: A case study of Wadi Madoneh in Jordan. Revista, Mexicana de Ciencias Geológicas 24(2): 185-193.

[8] Kouli M., Vallianatos F., Soupios P., DIMITRIS Alexakis D., 2006, A GIS example of Morphometric analysis in tectonic structures of Western Crete, Greece, 5th WSEAS International Conference on Environment, Ecosystems and Development.

[9] Cheng, Q., Ko, C., Yuan, Y., Ge, Y., Zhang, S., 2006, GIS modelling for predicting river runoff volume in ungauged drainages in Greater Toronto Area, Canada. Computers and Geosciences, 32: 1108-1119.

[10] Kumar, A., Singhal, M. K., 1999, Hydropower assesment for small ungauged catchments in Himalayan Region using GIS techniques. Workshop on GIS Applications in Power Sector Map India.

[11] Saraf, A. K., Kumar, A., 2006, Spatial technologies in Himalayan small hydropower development. Himalayan Small Hydropower Summit. October 12-13. Dehradun.

[12] Coskun, H.G., Alganci, U., Usta, G., 2008, Analysis of Land Use Change and Urbanization in the

Kucukcekmece Water Basin (Istanbul, Turkey) with Temporal Satellite Data using Remote Sensing and GIS, *Sensors*, 8 (11): 7213-7223.

[13] Coskun, H. G., 2009, Remote Sensing and GIS Techniques for Temporal Evaluation of Environmental Impacts on Major Drinking Water Dam and Basin of Metropolis Istanbul, *Fresenius Environmental Bulletin*, 18(3): 261 - 269, Parlar Scientific Publications

[14] Coskun, H. G., Alparslan, E., 2009, Environmental Modelling of Omerli Catchment Area in Istanbul, Turkey Using Remote Sensing and GIS Techniques, *Environmental Monitoring and Assessment*, 153(1-4):323-332.

[15] Goovaerts P., 2000, Geostatistical approaches for incorporating elevation into the spatial interpolation of rainfall. *J Hydrol* 228:113–129

[16] Lloyd C. D., 2005, Assessing the effect of integrating elevation data into the estimation of monthly precipitation in Great Britain. *J Hydrol* 308:128–150

[17] Cheng S. J., Hsieh HH, Wang Y. M., 2007, Geostatistical interpolation of space–time rainfall on Tamshui River basin, Taiwan. *Hydrol Process* 21:3136–3145

[18] Boroujerdy P. K., 2008, The analysis of precipitation variation and quantiles in Iran, 3rd IASME/WSEAS Int. Conf. on Energy & Environment, University of Cambridge, UK, February 23-25,

[19] Kok, A. L., Blais, J. A. R., Rangayyan, R. M., 1987, Filtering of digitally correlated gestalt elevation data. *Photogrammetric Engineering and Remote Sensing* 53 (5): 535-538.

[20] Ashe, R., 2003, Investigating runoff source area for an irrigation drain system using arc hydro tools, in *Proceedings of the Twenty-Third Annual ESRI User Conference*. San Diego.

[21] Atkinson, P. M. and Lloyd, C. D., 1998, Mapping precipitation in Switzerland with ordinary and indicator Kriging. *Journal of Geographic Information and Decision Analysis*, 2(2): 65-76.

[22] Nour, M. H., Smit D. W., Gamal El-Din M., 2006, Geostatistical mapping of precipitation: implications for rain gauge network design. *Water Science & Technology*, 53 (10): 101-110.

[23] Philips DL, Dolph J, Marks D., 1992, A comparison of geostatistical procedures for spatial analysis of precipitation in mountainous terrain. *Agric For Meteorol* 58:119–141

[24] Lloyd C. D., 2005, Assessing the effect of integrating elevation data into the estimation of monthly precipitation in Great Britain. *J Hydrol* 308:128–150

[25] Basistha A, Arya DS, Goel, N. K., 2008, Spatial Distribution of Rainfall in Indian Himalayas – A Case Study of Uttarakhand Region. *Water Resource Management* 22:1325–1346